Crystal structures and density functional theory calculations of *o*- and *p*-nitroaniline derivatives: combined effect of hydrogen bonding and aromatic interactions on dimerization energy

Kaisa Helttunen,[*,†] Lauri Lehtovaara,[†] Hannu Häkkinen,[†,‡] and Maija Nissinen[†]

Nanoscience Center, University of Jyväskylä, P.O. Box 35, FI-40014 Jyväskylä, Finland

E-mail: kaisa.j.helttunen@jyu.fi

Abstract

The interplay of strong and weak hydrogen bonds, dipole-dipole interactions and aromatic interactions of *o*- and *p*-nitroaniline derivatives was studied by combining crystal structure analysis and density functional theory (DFT) calculations. Crystal structures of four 2-nitroaniline derivatives, 2-((2-nitrophenyl)amino)ethyl methanesulfonate (**1A**), 2-((2-nitrophenyl)-amino)ethyl 4-methylbenzenesulfonate (**2A**), *N,N'*-((1,3-phenylenebis(oxy))bis(ethane-2,1-diyl))-bis(2-nitroaniline) (**3A**) and *N*-(2-chloroethyl)-2-nitroaniline (**4A**), and crystal structures of three 4-nitroaniline derivatives, 2-((4-nitrophenyl)amino)ethyl methanesulfonate (**1B**), 2-((4-nitrophenyl)amino)ethyl 4-methylbenzenesulfonate (**2B**) and *tert*-butyl-(2-((4-nitrophenyl)amino)-ethyl) carbonate (**5B**), were analyzed with regard to intra- and intermolecular hydrogen bonding and $\pi - \pi$ interactions. The effect of *o*/*p*-substitution on π-electron distribution, aromatic-

[*]To whom correspondence should be addressed
[†]Department of Chemistry
[‡]Department of Physics

ity of the nitroaniline ring and relative strength of intra- and intermolecular weak interactions were compared using HOMA indices, Hirshfeld surfaces and DFT calculations. The 2-nitroaniline derivatives contain an intramolecular hydrogen bond between amino and nitro groups creating a six-membered chelate ring, which formed pseudo-stacked structures with aromatic rings. Van der Waals corrected DFT calculations showed that stacking of a phenyl and a chelate ring contributed significantly to the dimerization of **1A** and **2A**. Therefore, it can be concluded that the phenyl-chelate interactions are important factor in stacking of the monomers in addition to C-H$\cdots$O hydrogen bonding. In 4-nitroaniline derivatives, intermolecular N-H$\cdots$O hydrogen bonds were in a significant role in packing, creating hydrogen bonded dimers in **1B** and **2B**, and hydrogen bonded chains in **5B**.

Introduction

Nitroaromatic compounds are widely used in industrial production of chemicals, such as explosives, pesticides, dyes and pharmaceuticals.[1] Nowadays, crystal forms of nitroarenes and nitroanilines are studied as potential organic non-linear optical (NLO) materials.[2] The environmental and biological effects of nitroarenes are significant. Nitroarenes pose toxic and mutagenic effects for organisms, which are further aggravated by the long life-time of nitroarenes in the environment due to resistance to oxidative attack.[3] In addition, biosynthesized nitroarenes bear important biological activities, for example, as antibiotics and in signalling.[4] In light of recently published data, these effects may rise from the aromatic interactions of nitroarenes with proteins.[5] Therefore, detailed understanding of the chemical nature of nitroarenes and their propensity to form weak interactions are useful in order to elucidate the biological activities and toxicity of nitro compounds and to develope new crystal materials for NLO applications.

In crystal engineering, complete understanding of weak intermolecular interactions in a crystal would be optimal for predicting the exact crystal packing and creating desired properties for crystalline materials. Over the years, the trend has been to look for weaker and weaker bonding forces to increase the understanding of complicated crystal packing and molecular recognition phenom-

ena. For example, halogen bonding[6] and weak C-H$\cdots$O hydrogen bonds, where C-H group acts as a hydrogen bond donor and oxygen as an hydrogen bond acceptor,[7,8] have been studied and used in crystal engineering of supramolecular complexes.[9] Many of these compounds have nitrobenzene functionality, since the oxygen atoms of the nitro group are good acceptors for weak hydrogen bonds.[10] The analysis of crystal structures of nitrobenzene and nitroaniline compounds reveals the abundancy of these bonds, which, in many cases, are important factors in crystal packing.[11] In addition, nitro groups form dipole-dipole interactions, which, depending on the geometry, form mainly by electrostatic interaction between negatively charged oxygens and positively charged nitrogens,[12] or may attain significant contribution from dispersion forces.[13]

Aromatic interactions have an important role in self-assembly and crystal packing of aromatic compounds. The role of π-stacking, edge-to-face π-stacking and weaker aliphatic C-H$\cdots\pi$ interaction in protein folding and small molecule binding into proteins have recently been illustrated.[5,14] Aromatic interactions are not easily controlled, and therefore, theoretical question about their origin, that is, whether they are governed by electrostatic or dispersion forces, have been investigated by computational and experimental methods.[15–18] There is strong evidence that π-stacking is dominated by dispersion forces.[15–17] Nevertheless, electrostatic component may be used to predict the binding energy.[18] Electron density withdrawing substituents, such as nitro group, polarize the π-electron cloud of the benzene ring,[19] and consequently, influence optimal geometry of the $\pi-\pi$ -interactions. For example, nitrobenzene dimers prefer slipped-parallel (offset face-to-face) orientation over T-shaped (edge-to-face) geometry (Figure 1), which is most stable for benzene dimers.[17]

In crystal structures, nitro groups are usually coplanar with the phenyl ring.[20] Possible explanation could be resonance coupling between the nitro group and the aromatic ring as indicated in the quinonoid structure (Figure 2). However, the lack of correlation between C–N bond lengths and coplanarity of the nitro group does not support this hypothesis.[21] In addition, NMR and computational analysis have shown for *para* substituted nitrobenzenes, such as 4-nitroaniline, that the nitro group withdraws a constant amount of electron density from the ring regardless of the presence

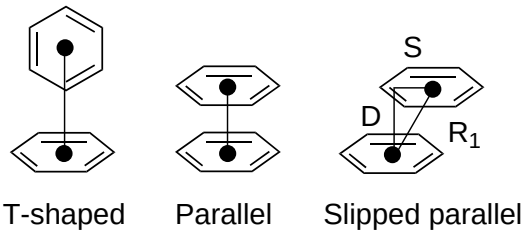

Figure 1: Classification of π-stacking geometries. Parameter R_1 is centroid-centroid distance, D is interplanar distance, and S is shift or centoid-centroid distance projected to a phenyl ring plane. T-shaped π-interaction is also known as edge-to-face, and parallel and slipped parallel as face-to-face and offset face-to-face π-interaction.

of electron density donating substituents.[22] These findings suggest that the resonance of the nitro group and the benzene ring are not strongly coupled, and the planar geometry is mainly caused by rotation barrier around C–N bond or crystal packing.[21] On the other hand, the electron deficient nitrophenyl ring accepts more readily the lone pair of the amino substituent, which enhances the input of quinonoid structure in the resonance hybrid of nitroanilines. Also substitution geometry creates differences in the electronic structure and aromaticity between *o*-, *m*- and *p*-nitroanilines.[23] *o*-Nitroaniline forms an intramolecular hydrogen bond between nitro and amino groups, which creates a six-membered chelate ring further extending the electron delocalization in the aromatic ring.

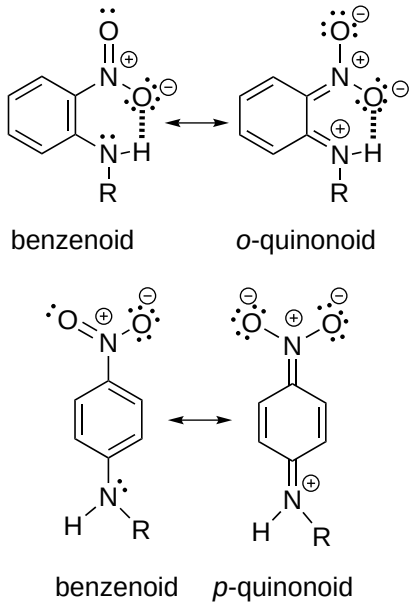

Figure 2: Benzenoid and quinonoid resonance structures for *o*- and *p*-nitroaniline showing intramolecular hydrogen bond of *o*-nitroaniline with a dashed bond.

During investigation of new supramolecular resorcinarene hosts,[24,25] seven 2-(nitrophenyl)-aminoethyl derivatives were prepared and crystallized. Analysis of the crystal structures opened up a possiblity to compare the effect of *ortho* (group **A**) versus *para* (group **B**) subsitution of nitroaniline rings on weak intra- and intermolecular interactions in crystal packing. Aniline N-H is the only strong hydrogen bond donor in the molecules, which formed intramolecular hydrogen bonded chelate rings in **1A**, **2A**, **3A** and **4A**, intermolecular hydrogen bonded rings in **1B** and **2B**, and chains in **5B**. In addition to the nitro groups, derivatives **1A**, **1B**, **2A** and **2B** contain sulfoxide, and **5B** a carbonate group as hydrogen bond acceptors. The derivatives contain one (**1A**, **1B**, **4A**, **5B**), two (**2A**, **2B**) or three (**3A**) aromatic rings, which creates a possibility for various intra- and intermolecular π-stacking geometries. Structures **2A**, **3A** and **4A** formed intermolecular parallel displaced π-stacking interactions, **1B** parallel and T-shaped π-interaction, **2B** intra- and intermolecular parallel π-stacking and intermolecular T-shaped π-interaction. Instead of π-stacking, structure **1A** formed dimers by stacking of chelate and phenyl rings.

Crystal packing and intermolecular interactions were analyzed using Hirshfeld surfaces and fingerprint plots.[26] Bond lengths and harmonic oscillation measure for aromaticity (HOMA)[27] were compared in order to elucidate differences between aromatic interactions of 2- and 4-nitroaniline derivatives. In addition, density functional theory was applied to the molecules and their dimers in order to understand how the substitution affects conformation, the π-stacking geometries, as well as, interplay of weak interactions in crystal packing. Taken together, these methods provide detailed and quantitative results about molecular conformation, strength of weak hydrogen bonds and π-stacking in nitroaniline crystals.

Experimental

Chemicals and solvents were obtained from commercial suppliers (Sigma-Aldrich and VWR) and used without further purification unless otherwise noted. Flash chromatography was performed with Combiflash Companion (Teledyne Isco) and Redisep Gold silica columns. NMR spectra

were recorded with a Bruker Avance DRX (500 MHz for ^{1}H and 126 MHz for ^{13}C) spectrometer at 30 °C. *J* values are given in Hz. ESI-MS spectra were measured with a Micromass LCT (ESI-TOF) instrument and EI-MS with a VG AutoSpec instrument using solid inlet. Melting points were determined with a Stuart Scientific SMP3 apparatus and are uncorrected. Elemental analyses were performed on a Vario EL III instrument.

Synthetic procedures

Preparation of **1A**,[24] **2A**,[25] **2B**[28] and **4A**[29] has been described elsewhere. See ESI for details.

2-((4-nitrophenyl)amino)ethyl methanesulfonate (**1B**): *p*-Nitro-*N*-(2-hydroxyethyl)-aniline[30] (1.00 g, 5.52 mmol) was dissolved in pyridine (3 ml), and methanesulfonyl chloride (0.51 ml, 6.59 mmol) was added dropwise into the solution at 0 °C (in ice bath) under nitrogen gas. The mixture was stirred at 0 °C for additional one hour, and 2.5 hours without ice bath. Water (50 ml) was added to the mixture. Yellow-brown precipitate was filtrated with suction and dried under vacuum. Product was recrystallized from hot chloroform-acetone-hexane solution to provide yellow crystals, yield 1.08 g (75 %). mp. 136-138 °C. ^{1}H NMR ($CDCl_3$, 500 MHz): 3.05 (s, 3H; CH_3), 3.62 (t, ^{3}J (H,H) = 5.2 Hz, 2H; CH_2), 4.44 (t, ^{3}J (H,H) = 5.2 Hz, 2H; CH_2), 6.60 (dt, ^{3}J (H,H) = 9.2 Hz, 2H; ArH), 8.12 (dt, ^{3}J (H,H) = 9.2 Hz, 2H; ArH) ppm. ^{13}C NMR ($CDCl_3$, 126 MHz): 37.9, 42.8, 67.2, 111.6, 126.6, 139.2, 152.4 ppm. Anal. Calcd for $C_9H_{12}N_2O_5S$: C, 41.53; H, 4.65; N, 10.76. Found: C, 41.53; H, 4.82; N, 10.84. m/z (EI) 260 M^+.

***N,N'*-((1,3-phenylenebis(oxy))bis(ethane-2,1-diyl))bis(2-nitroaniline)** (**3A**): A mixture of resorcinol (0.21 g, 1.89 mmol), Cs_2CO_3 (1.30 g, 4.00 mmol dried at 120 °C), dibenzo-18-crown-6 (0.14 g, 0.40 mmol) and dry acetonitrile (25 ml) was refluxed for 1 hour under nitrogen. A solution of 2-((2-nitrophenyl)amino)ethyl 4-methylbenzenesulfonate **2A** (1.23 g, 3.67 mmol) in 10 ml of dry acetonitrile was added dropwise, and the mixture was refluxed for two days. Dark brown mixture was filtrated and the solvent was distilled off under vacuum. Orange precipitate was dissolved in 70 ml of $CHCl_3$, washed four times with water and dried with $MgSO_4$. The product was purified using flash chromatography (SiO_2, $CHCl_3$ eluent with a gradient of 0-10 % MeOH containing 0.25

% triethylamine). Recrystallization from hot chloroform solution using hexane as an antisolvent provided orange crystals with 33 % yield (0.28 g). mp. 156.5-157 °C. ^{1}H NMR ($CDCl_3$, 500 MHz): 3.73 (q, ^{3}J (H,H) = 5.5 Hz, 4H; CH_2), 4.23 (t, ^{3}J (H,H) = 5.5 Hz, 4H; CH_2), 6.54 (t, ^{4}J (H,H) = 2.3 Hz, 1H; ArH), 6.57 (dd, ^{3}J (H,H) = 8.2 Hz, ^{4}J (H,H) = 2.4, 2H; ArH), 6.68 (m, 2H; ArH), 6.93 (dd, ^{3}J (H,H) = 8.7 Hz, 2H), 7.20 (t, ^{3}J (H,H) = 8.2 Hz, 1H; ArH), 7.46 (m, 2H), 8.19 (dd, ^{3}J (H,H) = 8.6 Hz, 2H; ArH), 8.31 (s, br, 2H; NH) ppm. ^{13}C NMR ($CDCl_3$, 126 MHz): 42.5, 66.3, 102.3, 107.9, 113.8, 115.9, 127.2, 130.3, 132.6, 136.3, 145.4, 159.8 ppm. Anal. Calcd for $C_{22}H_{22}N_4O_6 \cdot 0.55H_2O$: C, 59.94; H, 5.19; N, 12.50. Found: C, 58.58, H, 4.80; N, 12.66. m/z (ESI-TOF) 461 ($M + Na^+$), 477 ($M + K^+$).

***tert*-butyl (2-((4-nitrophenyl)amino)ethyl) carbonate (5B)**: *p*-Nitro-*N*-(2-hydroxyethyl)-aniline (0.27 g, 1.49 mmol) was dissolved in dry acetone (5 ml) under nitrogen gas. Di-*tert*-butyl dicarbonate (0.7 ml, 3.05 mmol) was added to the solution. The mixture was heated to 50 °C and stirred for 20 hours. At this stage only starting material was present in TLC (SiO_2, 99:1 $CHCl_3$:MeOH), whereupon more di-*tert*-butyl dicarbonate (0.7 ml, 3.05 mmol) was added. After 48 hours of stirring at 50 °C and three days at room temperature, solvent was distilled off under vacuum and the yellow residue was purified with flash chromatography to remove the excess dicarbonate (SiO_2, $CHCl_3$-MeOH 99:1). Recrystallization from hot chloroform solution using hexane as an antisolvent provided yellow block crystals with 34 % yield (0.14 g). mp. 144-145 °C. ^{1}H NMR ($CDCl_3$, 500 MHz): 1.49 (s, 9H; CH_3), 3.51 (t, ^{3}J (H,H) = 5.3 Hz, 2H; CH_2), 4.30 (t, ^{3}J (H,H) = 5.3 Hz, 2H; CH_2), 4.83 (s, br, 1H; NH), 6.56 (dt, ^{3}J (H,H) = 9.3 Hz, 2H; ArH), 8.09 (dt, ^{3}J (H,H) = 9.3 Hz, 2H; ArH) ppm. ^{13}C NMR ($CDCl_3$, 126 MHz): 27.9, 42.7, 64.9, 83.2, 111.4, 126.5, 138.8, 152.9, 153.6 ppm. Anal. Calcd for $C_{13}H_{18}N_2O_5$: C, 55.31; H, 6.43; N, 9.92. Found: C, 55.09; H, 6.36; N, 10.03. m/z (EI) 282 M^+.

Single crystal X-ray diffraction

Crystals of **1A** and **2A** were grown in $CHCl_3$ solution with hexane diffusion. Crystals of **1B**, **2B** and **3A** were grown in a NMR tube in $CDCl_3$ solution. Crystals of **4A** and **5B** were obtained

directly from the recrystallization in chloroform-hexane solution.

Single crystal X-ray data were recorded on a Nonius Kappa CCD diffractometer with Apex II detector using graphite monochromatized CuK_α (λ = 1.54178 Å) radiation at a temperature of 173 K. The data were processed and absorption correction was made to all structures with Denzo-SMN v.0.97.638.[31] The structures were solved by direct methods (SHELXS-97) and refined (SHELXL-97) against F^2 by full-matrix least-squares techniques using SHELX-97 software package[32] and Olex2.[33] The hydrogen atoms were calculated to their idealized positions with isotropic temperature factors (1.2 or 1.5 times the C temperature factor) and refined as riding atoms, except amine hydrogens, which were located from the Q-peaks and restrained using DFIX 0.91. Crystal structure analysis and figures were prepared using Mercury CSD 3.0,[34] and Olex2. Hirshfeld surfaces (plotted against d_{norm}, curvature and shape index) and 2D fingerprint plots were calculated using CrystalExplorer.[35] Crystallographic data (excluding structure factors) for the structures in this paper have been deposited with the Cambridge Structural Data Center as supplementary publication nos. CCDC 930277– 930283.

Powder X-ray diffraction

PXRD patterns of the nitroaniline derivatives were measured after recrystallization from chloroform-hexane solution using a PANalytical X'Pert Pro system in a reflection mode with monochromatized CuK_α radiation (λ = 1.54178 Å) at ambient temperature.

Computational

DFT calculations were performed using Turbomole program V6.4.[36,37] PBE exchange-correlation functional[38] with Grimme's van der Waals corrections[39] as implemented in Turbomole V6.4 were used. All calculations were performed with aug-cc-pVDZ basis.[40] The ground state geometries were fully optimized for **1A**, **1B**, **2A**, **2B** and *N*-ethyl-2-nitroaniline using crystallographic coordinates for isolated monomers and dimers as a starting point.

Results and discussion

Four 2-(2-nitrophenyl)aminoethyl derivatives (**1A**, **2A**, **3A**, **4A**) and three 2-(4-nitrophenyl)aminoethyl derivatives (**1B**, **2B**, **5B**) were prepared by nucleophilic substitution using standard synthetic methods (Figure 3). Compounds **1A**, **1B**, **2A** and **2B** have a sulfonyloxy group connected to the ethyl linker. Since **1A** and **1B** are *ortho* and *para* isomers of 2-((nitrophenyl)amino)ethyl methanesulfonate, comparison of their crystal structures reveals the effect of *o/p*-substitution on intra- and intermolecular weak interactions. The competing interactions are intra- and intermolecular strong hydrogen bonds from amino group, weak hydrogen bonds from aryl and alkyl C-H to nitro or sulfonyl oxygens, dipole-dipole interactions between nitro groups, and aromatic interactions between the nitroaniline rings. Compounds **2A** and **2B** contain an aromatic *p*-toluenesulfonyl group, which increases the possiblilities for intra- and intermolecular aromatic interactions. Dompounds **3A**, *N,N'*-((1,3-phenylenebis(oxy))-bis(ethane-2,1-diyl))bis(2-nitroaniline), has two 2-(2-nitrophenyl)-aminoethyl groups connected to a resorcinol ring, which reduces the number of available hydrogen bond acceptors and increases the number of aromatic rings. Compound **4A**, *N*-(2-chloroethyl)-2-nitroaniline, contains a ethyl chloride group, which induces C-H$\cdots$Cl hydrogen bonds and affects the acidity of -CH_2Cl protons. Compound **5B**, *tert*-butyl (2-((4-nitrophenyl)amino)ethyl) carbonate, contains a *tert*-butoxy carbonyloxy group in the 2-aminoethyl chain, which increases the ratio of aliphatic groups in the structure.

Crystal structures

The nitroaniline derivatives crystallized readily as yellow or orange crystals from chloroform or chloroform-hexane solution. Crystal structures of **1A**–**5B** were solved by single crystal X-ray diffraction (Tables 1 and 2). Powder X-ray diffraction patterns of the compounds were recorded to ensure that the single crystal structure was a good representative for the sample.[41]

The conformation of the nitroaniline ring in all derivatives was close to planar. The nitro group tilt angle from the phenyl ring plane was 2.9° in **1A**, 7.8° in **2A**, 4.5° in **3A** and 5.7° in **4A**. In

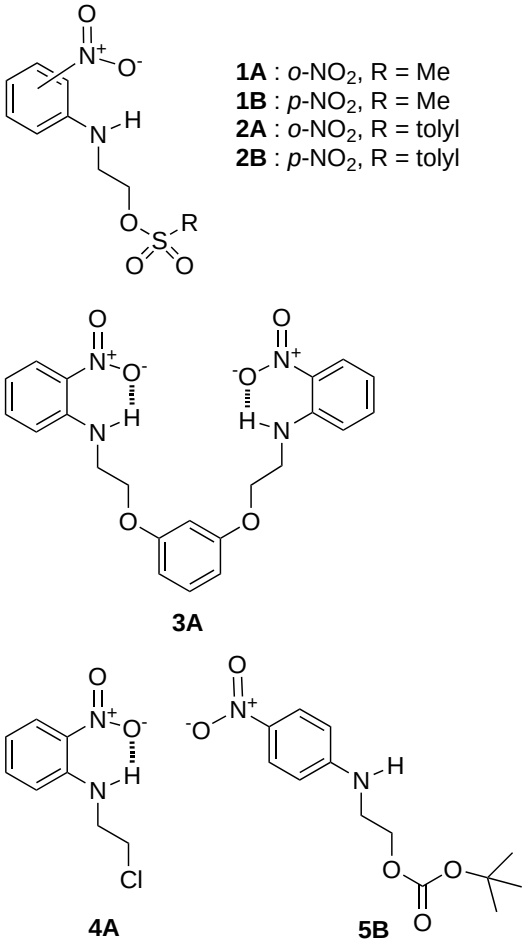

Figure 3: Nitroarene derivatives **1A**-**5B**. Group **A** compounds have 2-nitroaniline ring and intramolecular N-H$\cdots$O hydrogen bond (dashed bond), group **B** contains 4-nitroaniline derivatives.

Table 1: Crystal data and refinement parameters 1

Parameter	**1A**	**1B**	**2A**	**2B**
Composition	$C_9H_{12}N_2O_5S$	$C_9H_{12}N_2O_5S$	$C_{15}H_{16}N_2O_5S$	$C_{15}H_{16}N_2O_5S$
FW	260.27	260.27	336.36	336.36
Crystal system	Monoclinic	Monoclinic	Monoclinic	Monoclinic
Space group	$P2_1/c$	$P2_1/c$	$P2_1/c$	$P2_1/c$
a /Å	6.791(6)	13.1886(2)	7.9887(4)	9.2567(1)
b /Å	13.527(4)	10.2790(1)	27.077(2)	18.5024(2)
c /Å	12.462(2)	8.3635(1)	7.0718(5)	9.7785(1)
β/°	98.507(14)	97.1700(1)	94.729(5)	113.6710(1)
Volume /Å^3	1132.1(11)	1124.94(2)	1524.5(2)	1533.87(3)
Z	4	4	4	4
D_{calcd} /Mg·m^{-3}	1.527	1.537	1.466	1.457
F(000)	544	544	704	704
μ /mm^{-1}	2.704	2.721	2.150	2.137
Crystal size /mm	0.40 × 0.24 × 0.10	0.15 × 0.10 × 0.05	0.24 × 0.18 × 0.10	0.40 × 0.20 × 0.20
Meas. reflns	5800	2884	3944	4714
Indep. reflns	1980	1895	2630	2626
R_{int}	0.0592	0.0688	0.0306	0.0514
R_1 [$I > 2\sigma(I)$]	0.0352	0.0584	0.0404	0.0491
wR_2 [$I > 2\sigma(I)$]	0.0902	0.1533	0.1007	0.1270
R_1 (all data)	0.0387	0.0749	0.0498	0.0604
wR_2 (all data)	0.0930	0.1629	0.1070	0.1359
GooF on F^2	1.048	1.148	1.049	1.052
Largest diff. peak and hole /e Å^{-3}	0.34, -0.32	0.44, -0.34	0.25, -0.29	0.26, -0.47

Table 2: Crystal data and refinement parameters 2

Parameter	**3A**	**4A**	**5B**
Composition	$C_{22}H_{22}N_4O_6$	$C_8H_9ClN_2O_2$	$C_{13}H_{18}N_2O_5$
FW	438.44	200.62	282.29
Crystal system	Monoclinic	Monoclinic	Monoclinic
Space group	C2/c	$P2_1/c$	$P2_1/c$
a /Å	14.6336(2)	7.2248(1)	11.9007(1)
b /Å	7.2215(1)	16.2084(2)	16.0041(2)
c /Å	19.5363(2)	7.5660(1)	7.3763(1)
β/$^\circ$	105.2750(1)	94.4680(1)	94.3870(1)
Volume /Å^3	1991.59(4))	883.30(2)	1400.77(3)
D_{calcd} /Mg·m^{-3}	1.462	1.509	1.339
Z	4	4	4
F(000)	920	416	600
μ /mm^{-1}	0.905	3.586	0.870
Crystal size /mm	0.50 × 0.30 × 0.10	0.25 × 0.15 × 0.10	0.25 × 0.20 × 0.15
Meas. reflns	2621	2338	3944
Indep. reflns	1749	1508	2402
R_{int}	0.0337	0.0341	0.0689
R_1 [$I > 2\sigma(I)$]	0.0392	0.0415	0.0572
wR_2 [$I > 2\sigma(I)$]	0.1011	0.1080	0.1522
R_1 (all data)	0.0446	0.0464	0.0673
wR_2 (all data)	0.1053	0.1124	0.1614
GooF on F^2	1.057	1.065	1.043
Largest diff. peak and hole /e Å^{-3}	0.17, -0.23	0.19, -0.28	0.22, -0.29

4-nitroaniline derivatives, the nitro group tilt was smaller, 0.7° in **1B**, 3.3° in **2B** and 1.4° in **5B**. Visual inspection of the structures revealed that the small inclination of the nitro group is caused in most cases by weak hydrogen bonds to nitro oxygens, such as in **2A**, **2B**, **3A** and **4A**.

The amino nitrogen resides coplanary to the phenyl ring (1.5–7.9° tilt), which denotes a sp^2 hybridization. The torsion of the amino group hydrogen against C=C bond of the aromatic ring (C=C-N-H torsion) varies between 1.4–8.4°. In **2B**, however, a larger torsion angle of -19.5° was observed, resulting from the intermolecular hydrogen bond to sulfonyl oxygen.

All 2-nitroaniline derivatives (**A**) formed an intramolecular $S_1^1(6)$ N-H$\cdots$O-N hydrogen bond,[42] in which the D$\cdots$A distance is 2.62–2.63 Å (Figures 4 to 6). The 4-nitroaniline derivatives **1B** and **2B** (Figure 7) formed hydrogen bonded $R_2^2(14)$ dimers between amino hydrogens and sulfonyl oxygens. Compound **5B**, which does not contain a sulfonyloxy group, formed a hydrogen bonded $C_1^1(7)$ chain between amino hydrogen and nitro oxygen (Figure 8).

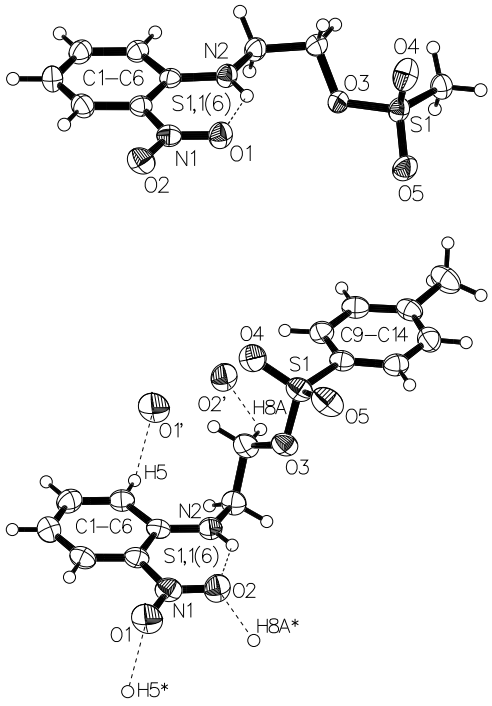

Figure 4: Crystal structures of **1A** (top) and **2A** (bottom) showing intramolecular $S_1^1(6)$ hydrogen bond and weak C-H$\cdots$O hydrogen bonds to nitro oxygens (H5$\cdots$O1 = 2.52 Å, 164°; H8A$\cdots$O2 = 2.62 Å, 137°), thermal ellipsoids at 50 % probability. Weak hydrogen bonds to sulfonyl oxygens not shown.

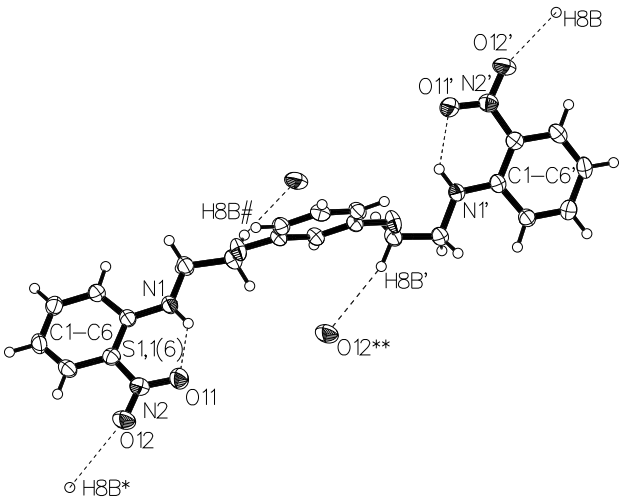

Figure 5: Crystal structure of **3A** showing intramolecular $S_1^1(6)$ hydrogen bond and weak C-H$\cdots$O hydrogen bond to nitro oxygen (H8B$\cdots$O12 = 2.67 Å, 163°), thermal ellipsoids at 50 % probability.

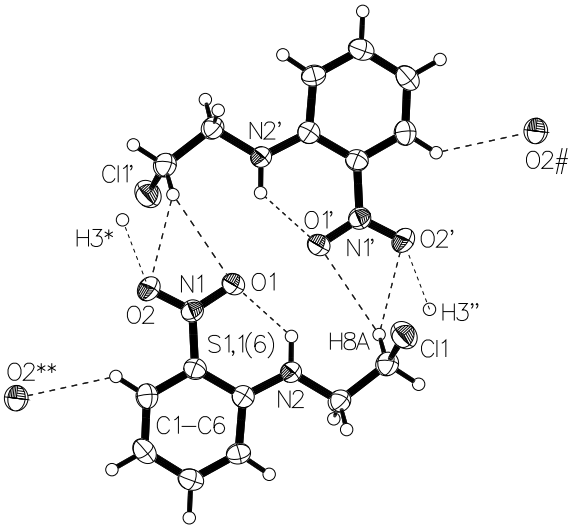

Figure 6: Crystal structure of **4A** formed dimers by weak C-H$\cdots$O hydrogen bonds to nitro oxygens: H8A$\cdots$O2 =2.57 Å, 148°; H8A$\cdots$O1 = 2.71 Å, 144°; H3$\cdots$O2 = 2.54 Å, 131°. Thermal ellipsoids at 50 % probability, Cl$\cdots$H contacts not shown.

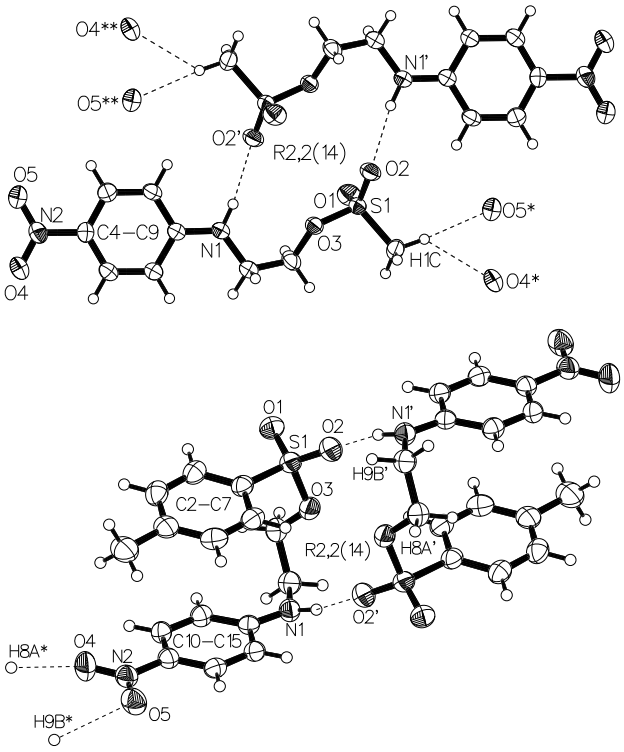

Figure 7: Crystal structures of **1B** (top) and **2B** (bottom) formed hydrogen bonded $R_2^2(14)$ dimers. Selected hydrogen bonds for **1B**: N1···O2 = 2.99 Å, <DHA 171°; H1C···O4 = 2.70 Å, 133°; H1C···O5 = 2.61 Å, 166°; for **2B**: N1···O2 = 2.99 Å, 159°. Thermal ellipsoids drawn at 50 % probability, weak hydrogen bonds to sulfonyl oxygens not shown.

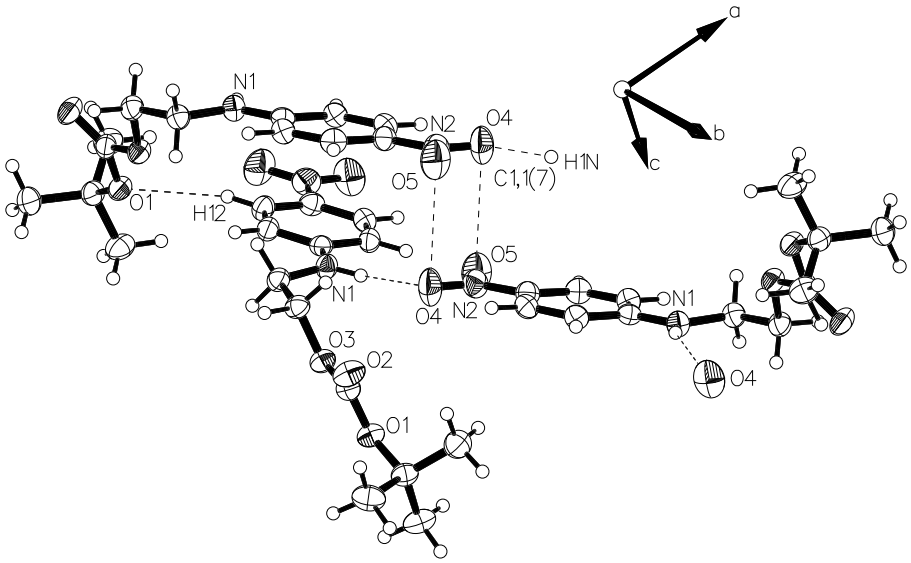

Figure 8: Crystal packing of **5B** showing $C_1^1(7)$ hydrogen bond pattern between amino and nitro groups (N1···O4 = 3.17 Å, 152°), H12···O1 contact (2.54 Å, 154°) and dipole-dipole interaction (N2···O4 = 3.35 Å, N2···O5 = 3.52 Å). Thermal ellipsoids drawn at 50 % probability.

Weak hydrogen bonds for nitro oxygens affect crystal packing of **1B**, **2B** and **4A**. A bifurcated C-H$\cdots$O bond, which is relatively common hydrogen bonding pattern in nitro compounds,[43] connects molecules of **1B** in chains and molecules of **4A** in dimer pairs.

The proportion of different short contacts within each crystal were compared using Hirshfeld surfaces and decomposed fingerprint plots. The relative surface area covered by C$\cdots$C, C$\cdots$H, H$\cdots$H and O$\cdots$H contacts (Figure 9) revealed the influence of aromatic face-to-face stacking, aromatic edge-to-face stacking, dispersion forces, and hydrogen bonds to the crystal packing. In **1A**, only 0.5 % of the surface area is involved in C$\cdots$C contacts indicating the lack of aromatic face-to-face stacking. Instead, hydrogen bonds cover almost half of the surface area (48.4 %) being the most significant contributor to the crystal packing. The fingerprint plots (Figure 10) show the contribution and bond distances and O$\cdots$H contacts in **1A**, **1B**, **2A** and **2B**. Most prominent features of **2A** are the proportion of C$\cdots$C contacts (9.1 %) and a narrow shape of fingerprint plot indicating the importance of π-stacking and lack of of edge-to-face π-interactions in crystal packing. The Hirshfeld surface of **3A** contains a significant proportion of C$\cdots$H contacts (16 %) resulting from aliphatic C-H$\cdots\pi$ interactions, whereas the role of aromatic interactions (C$\cdots$C contacts 5.3 %) is relatively small in comparison to nitroaniline derivatives with only one or two aromatic rings. Structure **4A** contains a significant proportion of Cl$\cdots$H contacts (17.9 %). In addition, the O$\cdots$H contacts play a significant role in packing, since the number of O$\cdots$H contacts per oxygen is high, even though the total surface area occupied by O$\cdots$H contacts is relatively low in comparison to other compounds (28.7 %). In **5B**, the proportion of H$\cdots$H contacts is larger than in the other structures due to input of *tert*-butyl group to the aliphatic dispersion forces.

Most of the nitroaniline derivatives formed at least one aromatic π-stacking interaction (Table 3). Compound **1B** formed a parallel π-interaction between two opposing molecules, and a T-shaped π-interaction to a π-stacked dimer above and below. Compound **2A** obtained a step-like conformation and formed continuous displaced parallel π-stacks of tolyl rings, and separate stacks for 2-nitroaniline rings (Figure 11). As in **1B**, the nitro and amino groups in the π-stacks are aligned in an antiparallel fashion. Compound **2B** adopted a clip-like conformation, in which the

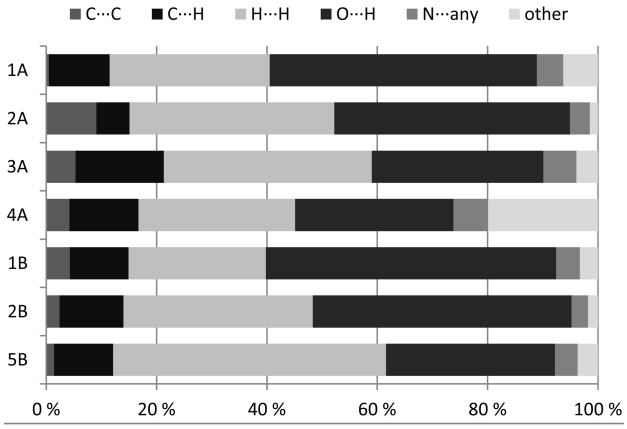

Figure 9: Short contact distribution of Hirshfeld surfaces.

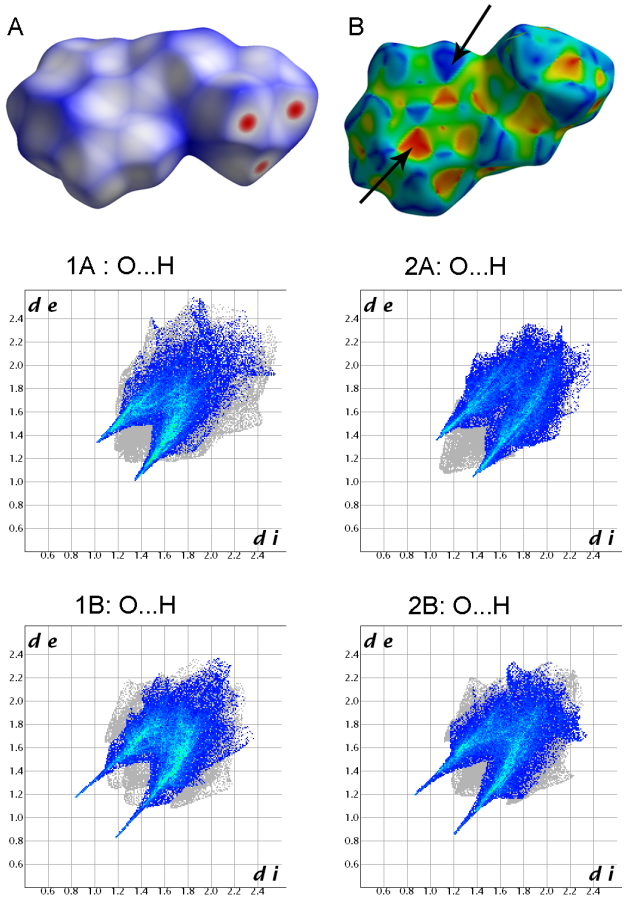

Figure 10: Hirshfeld surface of **1A** plotted against a) d_{norm} (red color indicates contacts shorter than vdW distance), b) shape index, arrows point to complementary patches. Fingerprint plots of **1A**, **1B**, **2A** and **2B** showing O···H contacts in color.

tolyl and 4-nitroaniline rings formed an intramolecular π-stack. The tolyl rings of two molecules further stacked in a displaced parallel geometry, and the 4-nitroaniline rings formed an edge-to-face π-interaction, in which a short contact between aryl C-H and nitro O5 has a significant role (Figure 12). Compounds **3A** and **4A** formed aromatic interaction between two 2-nitroaniline rings, again with an antiparallel orientation of the nitro and amino substituents.

Table 3: π-π stacking geometries in nitroaniline derivatives. R_1, R_2 = centroid-centroid distances, D = interplanar distance, S = shift.

Structure	Angle / °	D / Å	R_1 / Å	R_2 / Å	S / Å	Contact
1A	0.0	3.34	4.97	3.63	1.44	C1-C6···C1-C6 (1-x, 1-y, -z)
1B	0.0	3.51	3.53	-	0.44	C4-C9···C4-C9 (-x, -y, -z)
2A	0.0	3.44	3.84	3.53	1.70	C1-C6···C1-C6 (-x, 1-y, 1-z)
2A	0.0	3.43	3.78	3.83	1.59	C1-C6···C1-C6 (-x, 1-y, 2-z)
2A	1.6	3.45	3.63	-	1.12	C9-C14···C9-C14 (x, 1/2-y, -1/2+z)
2A	1.6	3.48	3.63	-	1.04	C9-C14···C9-C14 (x, 1/2-y, 1/2+z)
2B	11.0	3.69	3.85	-	1.10	C2-C7···C10-C15
2B	0.0	3.50	3.93	-	1.78	C2-C7···C2-C7 (1-x,-y,1-z)
3A	0.0	3.38	3.51	3.67	0.95	C1-C6···C1-C6 (1/2-x, -1/2-y, 1-z)
3A	0.0	3.30	4.71	3.59	1.23	C1-C6···C1-C6 (1/2-x, 1/2-y, 1-z)
4A	0.0	3.41	3.98	3.55	2.06	C1-C6···C1-C6 (-x, 1-y, 1-z)

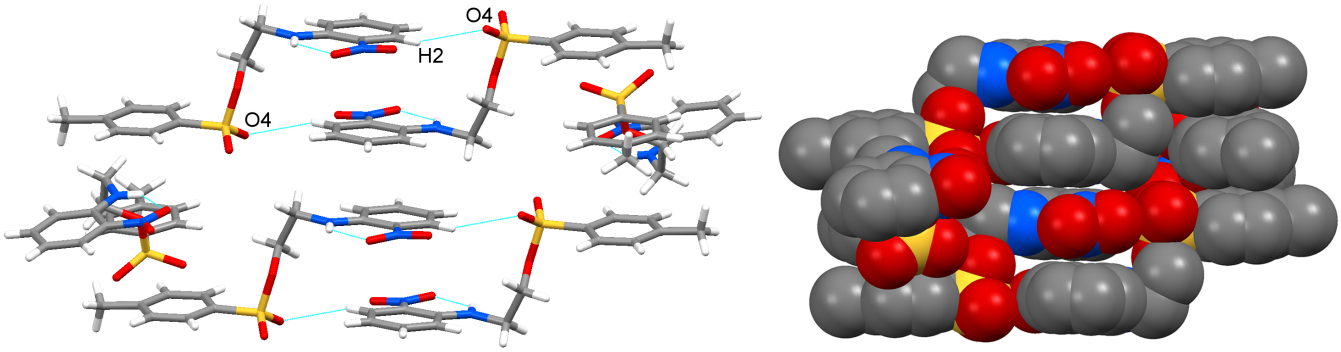

Figure 11: Aromatic interactions in crystal packing of **2A** shown as a stick (left) and a space-filling presentation (right, hydrogens omitted for clarity), H2···O4 = 2.62 Å, 149°.

1A and **5B** did not form aromatic interactions in a conventional geometry. In **1A**, the aromatic rings align as sheets, and on the one side the geometry seems favorable to dipole-dipole interaction between two nitro groups (Figure 13). On the other side, however, the Hirshfeld surface indicates flat and shape complementary areas between an aromatic ring of one molecule and an hydrogen

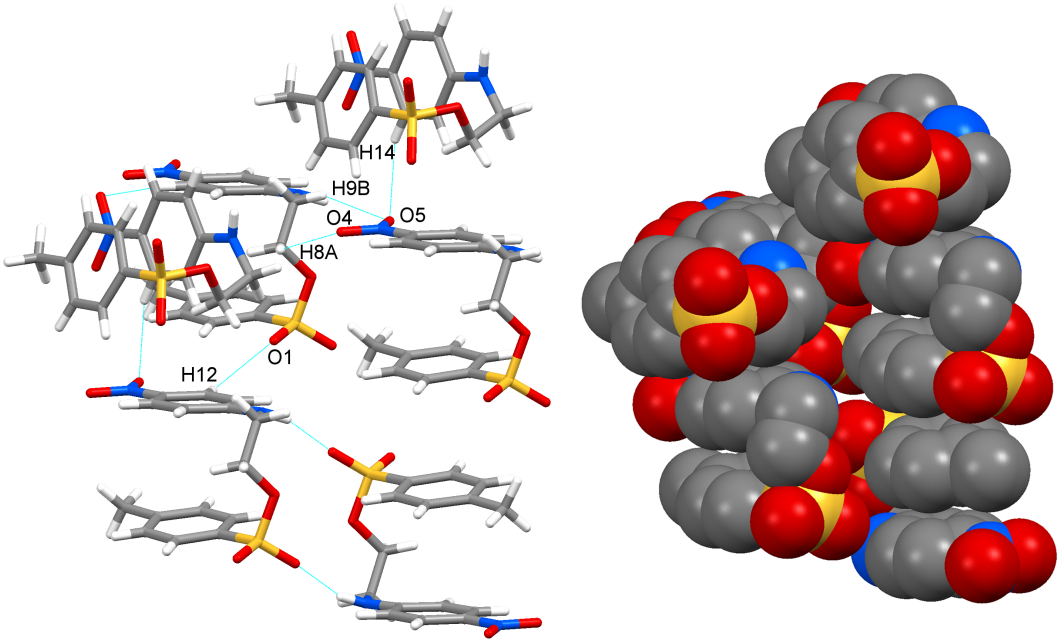

Figure 12: Crystal packing of **2B** as a stick (left) and a space-filling presentation (right, hydrogens omitted for clarity) showing aromatic interactions and hydrogen bonds; H9B···O5 = 2.49 Å, 150°; H8A···O4 = 2.62 Å, 129°, H14···O5 = 2.56 Å, 152°; H12···O1 = 2.58 Å, 125°.

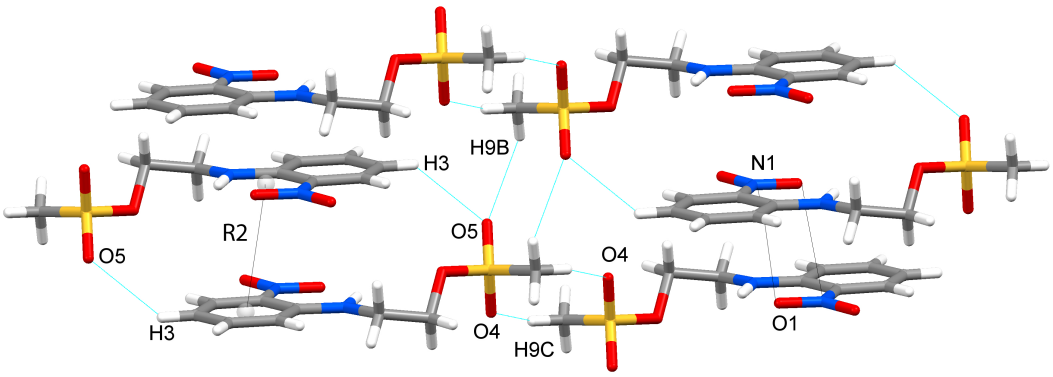

Figure 13: Crystal packing of **1A** showing weak hydrogen bonds, dipole-dipole interaction between O1 and N1 (3.38 Å) and phenyl and chelate ring stacking (R_2 = 3.63 Å).

bonded chelate ring of the other (Figure 10). The distance between the phenyl ring centroids, R_1, is too long for a aromatic interaction, whereas, the distance between the centroid of the chelate ring and centroid of the phenyl ring (R_2) is within bonding distance (first entry in Table 3). In **5B** the N-H group lies on top of the aromatic ring but the geometry does not remind an aromatic interaction, and overall, the position of the nitroaniline rings is more likely directed by the pairs of dipole-dipole interactions between the nitro groups (Figure 8).

Aromaticity of the nitroaniline rings

The substituent effects on the electron delocalization of the nitroaniline rings were analyzed by comparing C–C and C–N bond lengths. The $C-NO_2$ bond length was 1.44–1.45 Å for all derivatives, close to a typical C–N bond length for nitro substituent in a crystal structure, 1.47 Å.[44] The C–NH bond lengths were 1.35–1.37 Å, which correspond to a C–N bond to a planar sp^2 nitrogen showing that the amino nitrogen donates its lone pair to the aromatic π-electron system.

The aromaticity of the nitroaniline rings were compared using C–C bond lengths to calculate harmonic oscillation measure of aromaticity (HOMA) indices.[27] HOMA indice is calculated by summing the deviation of the observed bond lengths from ideal bond lengths (R_{opt}) and scaling the result to give HOMA = 0 for Kekulé type of structure and HOMA = 1 for completely delocalized structure with all bonds equal to R_{opt} = 1.388 Å.[45] The 2-nitroaniline derivatives had slight decrease in aromaticity in comparison to the 4-nitroaniline derivatives. The mean of HOMA indices for 2-nitroaniline derivatives was 0.88, and for 4-nitroaniline derivatives 0.93 (Table 4). Similar values have previously been obtained for *o*- and *p*-nitroaniline, 0.86 and 0.93, respectively,[23] and these values were close to the HOMA1 indices calculated for DFT optimized structures of **1A**, **1B**, **2A** and **2B**. In addition, the HOMA indice for the hydrogen bonded chelate ring in *o*-nitroaniline has previously been reported to be 0.59.[23] Similar calculation for group **A** derivatives gave a mean HOMA indice for chelate ring 0.67. In comparison to *o*-nitroaniline, the aromaticity of the chelate ring was slightly increased, which probably results from the inductive effect of the *N*-ethyl substituent.

Table 4: HOMA indices for crystal structures and DFT optimized structures of nitroaniline derivatives (HOMA1 = phenyl ring, HOMA2 = chelate ring).

Structure	HOMA1	HOMA2	HOMA1 (DFT)	HOMA2 (DFT)
1A	0.912	0.626	0.891	0.573
1B	0.934	-	0.947	-
2A	0.877	0.661	0.832	0.527
2B	0.936	-	0.914	-
3A	0.866	0.687	-	-
4A	0.859	0.686	-	-
5B	0.920	-	-	-

Recently, crystal structures of Schiff base salicylidene ligands suggesting a π-stacking interaction between a pseudo-aromatic ring formed through intramolecular hydrogen bonding and ordinary aromatic ring, have been published.[46,47] The chelate ring of 2-nitroaniline derivatives also show aromatic character based on the HOMA indices, even though the hydrogen bonded system is different lacking keto-enol tautomerism. Table 3 indicates that π-stacks of 2-nitroanilines contain shorter interplanar distances (D = 3.33–3.44 Å) than 4-nitroanilines (D = 3.50–3.51 Å). In addition, shortest interplanar distances, D < 3.40 Å, were connected with longest centroid–centroid distances, $R_1 > 4$ Å, and shortest phenyl and chelate centroid–centroid distances, $R_2 < 3.70$ Å, that is, stacking of the phenyl and chelate rings. A search of crystal structures in CSD revealed that the stacking of phenyl and chelate rings is present in many 2-nitroaniline compounds.[48] Considering the π-stacking geometries of 2-nitroaniline derivatives, especially in **1A**, and the aromatic character of the chelate ring, the interaction between phenyl ring and hydrogen bonded chelate ring was investigated using density functional theory calculations.

DFT calculations

Ground state energies and optimized geometries were calculated for compounds **1A**, **1B**, **2A** and **2B** starting from the crystal structure coordinates for isolated monomers and dimers in gas phase.

The optimized geometries of **1A**, **2A** and **2B** monomers were very close to the conformation in the crystal structure, indicating that monomers are in a relaxed conformation. In contrast,

optimized geometry of 4-nitroaniline monomer **1B** deviates from the crystal structure indicating that intermolecular interactions are required for sustaining the observed conformation. In crystal structure, the conformation of **1B** is linear and the monomers are connected into hydrogen bonded $R_2^2(14)$ dimer. When **1B** monomer was relaxed with DFT, it formed an intramolecular N-H$\cdots$O hydrogen bond to the sulfonyl oxygen. However, when **1B** dimer was relaxed with DFT, the intermolecular hydrogen bonds were re-established, and dimerization energy of -0.31 eV was obtained. Thus, intermolecular hydrogen bonds are stronger and likely improve the crystal packing into a regular structure, whereas intramolecular hydrogen bond may be weakened by molecular strain.

Although the **2B** monomers are nearly relaxed in the crystal, intermolecular hydrogen bonding and π-stacking stabilize the crystal. Based on DFT geometry optimizations, dimerization energy of $R_2^2(14)$ hydrogen bonded **2B** monomers is -0.87 eV, and dimerization energy of intermolecular tosyl-tosyl π-stacked **2B** monomers is -0.55 eV.

In order to calculate interaction energy for phenyl-chelate stacking, a dimer of **1A** molecules was relaxed starting from the crystal structure coordinates. The optimized geometry for the **1A** dimer is very similar to the original crystal structure geometry (Figure 14) having dimerization energy of -0.81 eV. The dimer is held together by two weak hydrogen bonds from aryl H3 to sulfonyl O5, and the proposed phenyl-chelate stacking interaction. The effect of weak hydrogen bonds on dimerization was eliminated by repeating optimization for a *N*-ethyl-2-nitroaniline dimer, which lacks the hydrogen bond acceptors. Dimerization energy for the relaxed structure is -0.62 eV. However, the stacking geometry is different than for the **1A** dimer. Therefore, we extracted a stacking geometry closely resembling the stacking geometry of the **1A** dimer from the geometry optimization path. This structure has dimerization energy of -0.53 eV. The energy difference of 0.09 eV between this partially relaxed structure and the optimal structure can be easily overcome by the hydrogen bonds. Moreover, the crystal structure and DFT optimized geometry of **2A** with dimerization energy of -0.65 eV is actually quite close to the fully relaxed structure of the *N*-ethyl-2-nitroaniline dimer. Thus, it can be concluded, that there is a binding interaction between the phenyl and chelate rings, which contributes significantly to stabilization of the **1A** and **2A** crystals.

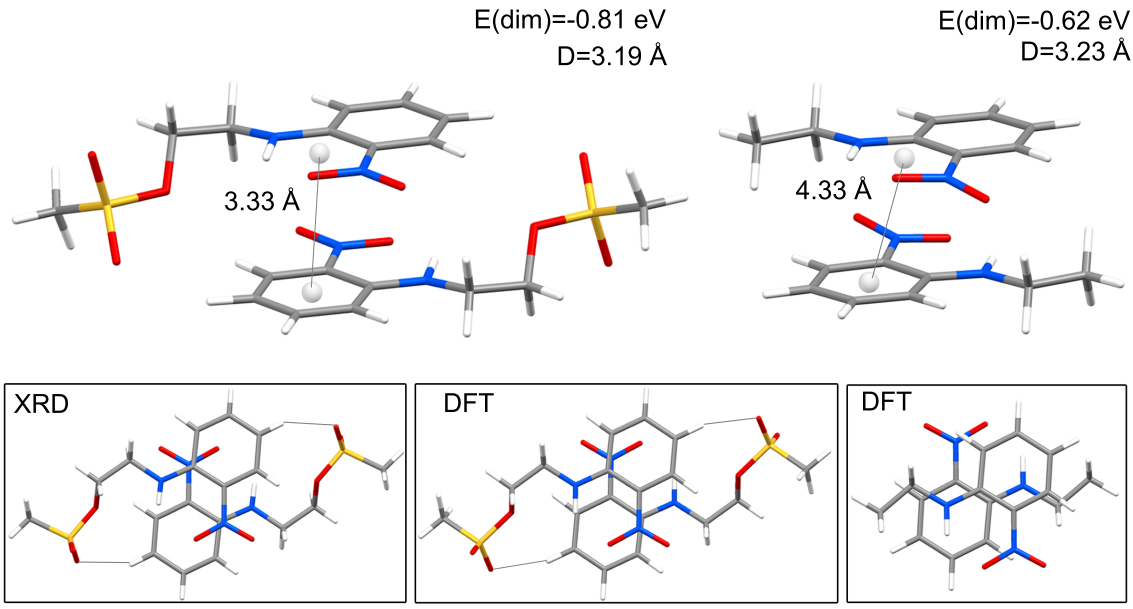

Figure 14: DFT optimized structures for **1A** dimer and *N*-ethyl-2-nitroaniline dimer. Top view of XRD structure and DFT structures.

Conclusion

The effect of *o*/*p*-substitution on intra- and intermolecular hydrogen bonds, dipole-dipole interactions and aromatic interactions in nitroaniline derivatives was investigated using crystal structure analysis and DFT calculations. Nitro and amino functionalities were approximately coplanar with the phenyl ring. The 2-nitroaniline derivatives formed an intramolecular hydrogen bond between amino and nitro groups creating a six-membered chelate ring, whereas in 4-nitroaniline derivatives, the amino hydrogen is sterically available for intermolecular hydrogen bonding. 4-Nitroaniline derivatives **1B** and **2B**, which contain sulfonyloxy groups, formed N-H$\cdots$O hydrogen bonded dimers. DFT calculations indicated that the hydrogen bonded dimer is more stable than an intramolecular hydrogen bond by -0.31 eV for **1B** and -0.87 eV for **2B**. In addition to strong hydrogen bonds, C-H$\cdots$O hydrogen bonds into sulfonyl oxygens and nitro oxygens were important in crystal packing for most derivatives, especially in **1A**, **1AB**, **2A**, **2B** and **4A**. Dipole-dipole interactions between nitro groups were in a minor role, and found only in structures **1A** and **5B**.

Differences in the shape and electron distribution between 2- and 4-nitroaniline rings creates

variation in π-stacking geometries. 2-nitroaniline derivatives had slightly lower aromaticity than 4-nitroaniline derivatives based on the HOMA indices. In 4-nitroaniline derivatives, parallel and T-shaped π-interactions were observed, whereas in 2-nitroaniline derivatives, parallel displaced π-stacking and phenyl-chelate stacking was abundant. Closer investigation of the 2-nitroaniline derivatives **1A** and **2A** using DFT, revealed that stacking of a phenyl and a chelate ring formed a weakly bonded dimer, in which, phenyl-chelate stacking contributed significantly to the dimerization energy. Thus, phenyl-chelate stacking may be regarded as a complementary interaction to phenyl-phenyl stacking, which affects crystal packing of 2-nitroaniline derivatives.

Acknowledgement

Emil Aaltonen foundation and Academy of Finland (project 21000019111) are acknowledged for funding. Ms. Mirja Lahtiperä is acknowledged for measuring the EI-MS spectra and Mr. Reijo Kauppinen for measuring the NMR spectra. Dr. Elisa Nauha is thanked for assistance with the XRD.

Supporting Information Available

NMR spectra and synthetic procedures, PXRD patterns, crystallographic tables, and figures for DFT optimized structures.

Notes and References

(1) (a) Ju, K.-S.; Parales, R. E. *Microbiol. Mol. Biol. Rev.* **2010**, *74*, 250–272; (b) Downing, R. S.; Kunkeler, P. J.; van Bekkum, H. *Catalysis Today* **1997**, *37*, 121–136.

(2) (a) Bailey, R. T.; Cruickshank, F. R.; Pavlides, P.; Pugh, D.; Sherwood, J. N. *Journal of Physics D: Applied Physics* **1991**, *24*, 135–145; (b) Wong, M. S.; Bosshard, C.; Günter, P. *Adv. Mater.* **1997**, *9*, 837–842; (c) Marder, S. R. *Chem. Commun.* **2006**, 131–134.

(3) (a) Purohit, V.; Basu, A. K. *Chem. Res. Toxicol.* **2000**, *13*, 673–692; (b) Friemann, R.; Ivkovic-Jensen, M. M.; Lessner, D. J.; Yu, C.-L.; Gibson, D. T.; Parales, R. E.; Eklund, H.; Ramaswamy, S. *J. Mol. Biol.* **2005**, *348*, 1139–1151.

(4) Winkler, R.; Hertweck, C. *ChemBioChem* **2007**, *8*, 973–977.

(5) Zhang, A. X.; Murelli, R. P.; Barinka, C.; Michel, J.; Cocleaza, A.; Jorgensen, W. L.; Lubkowski, J.; Spiegel, D. A. *J. Am. Chem. Soc.* **2010**, *132*, 12711–12716.

(6) (a) Politzer, P.; Murray, J. S. *ChemPhysChem* **2013**, *14*, 278–294; (b) Troff, R. W.; Mäkelä, T.; Topic, F.; Valkonen, A.; Raatikainen, K.; Rissanen, K. *Eur. J. Org. Chem.* **2013**, *2013*, 1617–1637.

(7) Desiraju, G. R. *Acc. Chem. Res.* **1991**, *24*, 290–296.

(8) Steiner, T. *Crystallogr. Rev.* **2003**, *9*, 177–228.

(9) (a) Pigge, F. C.; Ghasedi, F.; Zheng, Z.; Rath, N. P.; Nichols, G.; Chickos, J. S. *J. Chem. Soc., Perkin Trans. 2* **2000**, 2458–2464; (b) Reddy, C. M.; Reddy, L. S.; Aitipamula, S.; Nangia, A.; Lam, C.-K.; Mak, T. C. W. *CrystEngComm* **2005**, *7*, 44–52; (c) Kumar, V. S. S.; Pigge, F. C.; Rath, N. P. *Cryst. Growth Des.* **2006**, *6*, 193–196.

(10) (a) Sharma, C. V. K.; Panneerselvam, K.; Pilati, T.; Desiraju, G. R. *J. Chem. Soc., Perkin Trans. 2* **1993**, 2209–2216; (b) Sharma, C. V. K.; Desiraju, G. R. *J. Chem. Soc., Perkin Trans. 2* **1994**, 2345–2352.

(11) (a) Willey, G. R.; Drew, M. G. B. *Acta Crystallogr., Sect. C: Cryst. Struct. Commun.* **1985**, *C41*, 589–594; (b) Glidewell, C.; Low, J. N.; Skakle, J. M. S.; Wardell, S. M. S. V.; Wardell, J. L. *Acta Crystallogr., Sect. B: Struct. Sci.* **2004**, *B60*, 472–480; (c) Saeed, S.; Rashid, N.; Hussain, R.; Jones, P. G. *Acta Crystallogr., Sect. E: Struct. Rep. Online* **2009**, *E65*, o2106, So2106/1–So2106/8; (d) Collas, A.; Zeller, M.; Blockhuys, F. *Acta Crystallogr.,*

Sect. C: Cryst. Struct. Commun. **2011**, *C67*, o171–o174; (e) Paul, A.; Kubicki, M.; Jelsch, C.; Durand, P.; Lecomte, C. *Acta Crystallogr., Sect. B: Struct. Sci.* **2011**, *B67*, 365–378.

(12) Bertolasi, V.; Gilli, P.; Ferretti, V.; Gilli, G.; Vaughan, K.; Jollimore, J. V. *Acta Crystallogr., Sect. B: Struct. Sci.* **1999**, *B55*, 994–1004.

(13) (a) Wozniak, K.; He, H.; Klinowski, J.; Jones, W.; Grech, E. *J. Phys. Chem.* **1994**, *98*, 13755–13765; (b) Platts, J. A.; Howard, S. T.; Wozniak, K. *Chem. Phys. Lett.* **1995**, *232*, 479–485.

(14) Brandl, M.; Weiss, M. S.; Jabs, A.; Sühnel, J.; Hilgenfeld, R. *J. Mol. Biol.* **2001**, *307*, 357–377.

(15) il Kim, E.; Paliwal, S.; Wilcox, C. S. *J. Am. Chem. Soc.* **1998**, *120*, 11192–11193.

(16) Kamishima, M.; Kojima, M.; Yoshikawa, Y. *J. Comput. Chem.* **2001**, *22*, 835–845.

(17) Tsuzuki, S.; Honda, K.; Uchimaru, T.; Mikami, M. *J. Chem. Phys.* **2006**, *125*, 124304/1–124304/6.

(18) Watt, M.; Hardebeck, L. K. E.; Kirkpatrick, C. C.; Lewis, M. *J. Am. Chem. Soc.* **2011**, *133*, 3854–3862.

(19) Tonogaki, M.; Kawata, T.; Ohba, S.; Iwata, Y.; Shibuya, I. *Acta Crystallogr., Sect. B: Struct. Sci.* **1993**, *B49*, 1031–1039.

(20) Holden, J. R.; Dickinson, C.; Bock, C. M. *J. Phys. Chem.* **1972**, *76*, 3597–3598.

(21) Holden, J. R.; Dickinson, C. *J. Phys. Chem.* **1977**, *81*, 1505–1514.

(22) (a) Lipkowitz, K. B. *J. Am. Chem. Soc.* **1982**, *104*, 2647–2648; (b) Gawinecki, R.; Kolehmainen, E.; Dobosz, R. *Struct. Chem.* **2011**, *22*, 1379–1383.

(23) Zych, T.; Misiaszek, T.; Szostak, M. M. *Chem. Phys.* **2007**, *340*, 260–272.

(24) Helttunen, K.; Nauha, E.; Kurronen, A.; Shahgaldian, P.; Nissinen, M. *Org. Biomol. Chem.* **2011**, *9*, 906–914.

(25) Salorinne, K.; Weimann, D. P.; Schalley, C. A.; Nissinen, M. *Eur. J. Org. Chem.* **2009**, 6151–6159.

(26) (a) Spackman, M. A.; McKinnon, J. J. *CrystEngComm* **2002**, *4*, 378–392; (b) McKinnon, J. J.; Jayatilaka, D.; Spackman, M. A. *Chemical Communications* **2007**, 3814–3816; (c) Spackman, M. A.; Jayatilaka, D. *CrystEngComm* **2009**, *11*, 19–32.

(27) Krygowski, T. M. *J. Chem. Inf. Comput. Sci.* **1993**, *33*, 70–78.

(28) Rudesill, J. T.; Severson, R. F.; Pomonis, J. G. *J. Org. Chem.* **1971**, *36*, 3071–3076.

(29) (a) Karrer, P.; Naef, R. *Helv. Chim. Acta* **1936**, *19*, 1029–1033; (b) Ramage, G. R.; Trappe, G. *J. Chem. Soc.* **1952**, 4406–4409.

(30) *p*-Nitro-*N*-(2-hydroxyethyl)-aniline was prepared from commercially available 4-nitro-1-bromobenzene adapting the procedure described for *o*-nitro-*N*-(2-hydroxyethyl)-aniline by McManus, J.M.; Herbst, R.M. *J. Org. Chem.* **1959**, *24*, 1042-1043.

(31) Otwinowski, Z.; Minor, W. *Methods Enzymol.* **1997**, *276*, 307–326.

(32) Sheldrick, G. M. *Acta Crystallogr., Sect. A: Found. Crystallogr.* **2008**, *A64*, 112–122.

(33) Dolomanov, O. V.; Bourhis, L. J.; Gildea, R. J.; Howard, J. A. K.; Puschmann, H. *J. Appl. Crystallogr.* **2009**, *42*, 339–341.

(34) Macrae, C. F.; Edgington, P. R.; McCabe, P.; Pidcock, E.; Shields, G. P.; Taylor, R.; Towler, M.; van de Street, J. *J. Appl. Crystallogr.* **2006**, *39*, 453–457.

(35) Wolff, S. K.; Grimwood, D. J.; McKinnon, J. J.; Turner, M. J.; Jayatilaka, D.; Spackman, M. A. CrystalExplorer. 2012.

(36) TURBOMOLE V6.4 2012, a development of University of Karlsruhe and Forschungszentrum Karlsruhe GmbH, 1989-2007, TURBOMOLE GmbH, since 2007; available from `http://www.turbomole.com`.

(37) Ahlrichs, R.; Baer, M.; Haeser, M.; Horn, H.; Koelmel, C. *Chem. Phys. Lett.* **1989**, *162*, 165–169.

(38) Perdew, J. P.; Burke, K.; Ernzerhof, M. *Phys. Rev. Lett.* **1996**, *77*, 3865–3868.

(39) Grimme, S. *Journal of Computational Chemistry* **2004**, *25*, 1463–1473.

(40) Weigend, F.; Köhn, A.; Hättig, C. *J. Chem. Phys.* **2002**, *116*, 3175–3183.

(41) The PXRD diffraction patterns are published in the ESI, and they match well with the calculated pattern of the single crystal experiments. The deviation of the relative intensities from calculated pattern in **1A** probably result from the crystal morphology and small amount of sample available for the measurement.

(42) See for details of graph set symbols: Etter, M. C. *Acc. Chem. Res.* **1990**, *23*, 120–126.

(43) A search of CSD database V5.34 returned 950 bifurcated C-H$\cdots$O hydrogen bonds in nitro compounds.

(44) Allen, F. H.; Kennard, O.; Watson, D. G.; Brammer, L.; Orpen, A. G.; Taylor, R. *J. Chem. Soc., Perkin Trans. 2* **1987**, *0*, S1–S19.

(45) See Table 1 in Krygowski, T. M., *J. Chem. Inf. Comput. Sci.* **1993**, *33*, 70–78.

(46) Dutta, A.; Jana, A. D.; Gangopadhyay, S.; Das, K. K.; Marek, J.; Marek, R.; Brus, J.; Ali, M. *Phys. Chem. Chem. Phys.* **2011**, *13*, 15845–15853.

(47) *Acta Crystallogr. Sect. B.: Struct. Sci.* **2012**, *68*, 71–79.

(48) CSD V5.34 search for *N*-alkyl 2-nitroaniline motif with D < 3.8 Å returned 89 structures, which contain 112 π-stacking interactions and 30 phenyl-chelate stacking geometries. In

addition, 40 out of 112 π-stacking interactions may have contribution from phenyl-chelate stacking ($R_2 < R_1$).

This material is available free of charge via the Internet at `http://pubs.acs.org/`.

For Table of Contents use only

Crystal structures and density functional theory calculations of *o*- and *p*-nitroaniline derivatives: combined effect of hydrogen bonding and aromatic interactions on dimerization energy

Kaisa Helttunen, Lauri Lehtovaara, Hannu Häkkinen, and Maija Nissinen

Graphical abstract:

Interplay of weak hydrogen bonds and phenyl-chelate stacking revealed by applying density functional theory on crystal structures of nitroaniline derivatives.